



Research Paper

CO gas sensitivity and its oxidation over TiO₂ modified by PANI under UV irradiation at room temperature

Zhongming Wang^{a,b}, Xiaoying Peng^{a,b}, Chuyun Huang^{a,b}, Xun Chen^a, Wenxin Dai^{a,b,*}, Xianzhi Fu^{a,*}

^a Research Institute of Photocatalysis, State Key Laboratory of Photocatalysis on Energy and Environment, Fuzhou University, Fuzhou, 350002, China

^b Key Laboratory of Eco-materials Advanced Technology (Fuzhou University), Fujian Province University, Fuzhou, 350002, China

ARTICLE INFO

Article history:

Received 26 April 2017

Received in revised form 25 June 2017

Accepted 26 July 2017

Available online 28 July 2017

Keywords:

PANI modified TiO₂

Carbon monoxide

Photo-assisted gas sensitivity

Photocatalytic oxidation

ABSTRACT

A series of polyaniline–titanium dioxide (PANI/TiO₂) nanocomposite film sensor were fabricated by an in-situ chemical oxidation polymerization of aniline at TiO₂ (anatase) surface, and were evaluated the CO gas sensitivity under UV irradiation at room temperature. Although adding PANI into TiO₂ seemed to weaken the photo-assisted conductivity of film sensor sample at N₂ atmosphere, it enhanced the photo-assisted gas sensitivity to CO. Based on the chemical characterization results of PANI/TiO₂ by FT-IR, Raman and XPS, it is proposed that the protonated N site in PANI chains (formed by TiO₂ interacting with PANI) would promote the adsorption of CO, resulting in the more electrons from CO to PANI by the typical π-conjugated structures of benzenoid and quinonoid units and then to TiO₂ by the hydrogen bonds (N···H···O) in the interface of PANI and TiO₂. Moreover, the presence of H₂O could enhance this photo-assisted gas sensitivity. Furthermore, the PANI/TiO₂ powder sample also exhibited a higher activity of photocatalytic oxidizing CO than the pure TiO₂ sample, indicating that the enhancement in the photo-assisted sensing response to CO would benefit the photocatalytic oxidation of CO over PANI/TiO₂. This study not only provides a possible approach to develop a photo-assisted gas-sensitive material by introducing the structure of organic-inorganic hybridized nanocomposite, but also provides a possible method to estimate the photocatalytic activity of a semiconductor material by testing its photo-assisted sensitivity to the reactant gas.

© 2017 Elsevier B.V. All rights reserved.

1. Introduction

Semiconductor metal oxides, such as SnO₂ [1], TiO₂ [2], ZnO [3], WO₃ [4], CeO₂ [5] have been widely studied in gas sensors because of the prominent advantages of high sensitivity, good stability and fast response. However, these materials are usually applicable at high operating temperature, which resulted in higher power consumption and also being inapplicable for detecting explosive gases. In recent years, conducting polymers, with unique physical and chemistry properties as well as versatility and processability [6–9], have also extensively studied in gas sensor, biological sensing, chemcial sensor [10–12]. Among the host of conducting polymers is polyaniline (PANI, with a typical π-conjugated structure), regarded as a promising candidates in the past decades owing to its high con-

ductivity, good stability in the air [13], facile fabrication [14], low cost, high redox reversibility [15], and controllability of the electrical properties [16]. Although conducting polymer gas sensors can be applicable for the different target gases at room temperature [17], they were also confronted with some problems, such as a relatively low sensitivity and an unsatisfying stability [18].

To improve the gas sensing property of a single semiconductor oxide or conducting polymer, various composites of conducting polymer with inorganic nanoparticles have been synthesized to fabricate polymer/inorganic nanocomposite sensors [19–22]. For example, Ram et al. [23] have studied the property of a self-assembled PANI/TiO₂ or PANI/SnO₂ ultrathin film for CO gas sensing. Wang et al. [24] used Core–Shell CeO₂ Nanoparticles@Cross-linked PANI with p–n heterojunctions to enhance sensitivity and stability of room-temperature NH₃ sensors. A polyaniline/In₂O₃ nanofiber composite sensor for H₂, CO and NO₂ gas sensing application has been developed by Sadek et al. [25]. In addition, Nasirian et al. [26] have investigated gas sensing mechanism of hydrogen based on polyaniline/anatase titania nanocomposite. These composite materials not only can take

* Corresponding authors at: Research Institute of Photocatalysis, State Key Laboratory of Photocatalysis on Energy and Environment, Fuzhou University, Fuzhou, 350002, China.

E-mail addresses: daiwenxin@fzu.edu.cn (W. Dai), xzfu@fzu.edu.cn (X. Fu).

all advantages of the properties of conductive polymer and inorganic particles, but maybe also own synergetic or complementary behaviors as a new kind of composite materials.

Light illumination as considerable efforts have also been devoted to enhance the gas sensitivity and decrease the response temperature over the semi-conductor sensors to a great extent [27,28]. Due to its ultraviolet (UV) light response property, semiconductor have been widely investigated for the photo-assisted gas sensitivity over the past two decades [29,30]. For PANI/TiO₂, considering that the carrier transport may be conducted on account of a good energy band gap matching between TiO₂ (the positions of the valence band and conduction band) and PANI chains (the lowest unoccupied molecular orbital level (LUMO) and highest occupied molecular orbital (HOMO) in the benzenoid and quinonoid units) with the formation of the localized states in their junction [31], introducing UV light maybe benefits to the electron transfer in the interface of PANI/TiO₂ and then enhance its sensing response to gas.

Moreover, our previous works have found that the photocatalytic oxidation of a reactant over TiO₂ not only depends on the formation of the photo-generated carriers and the subsequent activated oxidizing species, but maybe also depends on the electron transfer behavior at the interface of the adsorbed reactant and TiO₂ [32]. This indicates that the enhancement in the photo-assisted sensing response of a semiconductor sensor to a reactant can promote the subsequent photocatalytic oxidation of the reactant over this semiconductor. With this viewpoint, we think that the introduction of PANI can not only enhance the photo-assisted gas sensing properties of TiO₂, but maybe also promote the photocatalytic performance.

Therefore, in this work, we have prepared a polyaniline titanium dioxide (PANI/TiO₂) nanocomposite, and investigated its CO gas sensing property under UV irradiation. It was expected that the photo-generated electrons by TiO₂ excitation could transfer along the interface of PANI/TiO₂, and enhance the gas sensitivity. As we hoped, an appropriate content of PANI added into TiO₂ did promote the gas sensitivity to CO under UV irradiation. Moreover, the PANI/TiO₂ also exhibited a better photocatalytic oxidizing CO than TiO₂.

2. Experimental

2.1. Preparation of materials

The PANI/TiO₂ nanocomposite was prepared by in-situ chemical oxidative polymerization method [33]. In a typical procedure, 0.5 g commercial TiO₂ powder with average size of 5–10 nm (>99.9% purity, Aladdin,) was dispersed in 50 mL deionized water in a 100 mL beaker, then a certain amount of aniline (99.5% purity, Shanghai Chengjie Chemistry Co. Ltd, China) was joined in above solution with a burette under magnetic stirring for 30 min. Then designated amounts of (nominal molar ratio of 0.01 mol L⁻¹ ammonium persulfate (NH₄)₂S₂O₈ (APS, 99.8% purity, Aladdin) with an equal molar ratio to aniline were then slowly dropwise into the above suspension with constant stirring. Successive polymerization for 12 h was to obtain PANI/TiO₂ composite deposition. The precipitate of PANI/TiO₂ composite was removed by filtration, centrifugation, washed repeatedly by deionized water. At last, the different contents (2.0 wt%, 4.0 wt%, 6.0 wt% and 8.0 wt% ratios of PANI to TiO₂) of PANI/TiO₂ nanocomposites was obtained after dried at 80 °C for 12 h.

Note that the ratios of PANI to TiO₂ in these prepared samples actually expressed the ratios of the added aniline into TiO₂ during the preparing process. This is because the molecular weight of PANI polymerized by aniline is unknown, resulting in the PANI content

not being calculated by the added aniline. To determine the contents of PANI in different PANI/TiO₂ samples, the ratio of the added aniline into TiO₂ was used to represent the ratio of PANI to TiO₂. In fact, not all the added aniline could be polymerized into PANI during the above preparing process. The elemental analysis result (Vario EL Cube) showed that the mass fraction of N in the 4% PANI/TiO₂ sample was about 0.3 wt%, corresponding to aniline content about 2.0 wt% (almost a half aniline maybe lost).

2.2. Fabrication of PANI/TiO₂ nanocomposite film sensor device

The sensor device was fabricated by the following process in our previous report [29,34]. A commercial alumina sheet (1.5 cm × 1 cm) with a comb-like gold electrode (also called interdigitated gold electrode) on one side surface which gap size was 0.15 mm was used as the substrate for sensors. Firstly, the interdigitated gold electrode sheet was pretreated by ultrasonic treatment with ethanol (99.7% purity) and deionized water in sequence and dried in oven. Then, a 50 μL nanoparticle suspension {30 mg of above prepared PANI/TiO₂ powder was dispersed into a 1 mL terpineol (Shanghai Chengjie Chemistry Co. Ltd, China) solvent} was dropped onto the surface of the comb-like gold electrode. This substrate was dried at 100 °C for 1 h and then calcined in air at 350 °C for 3 h with a heating rate 2 °C min⁻¹ in a muffle. After cooling down to room temperature naturally, the gas sensor device was obtained. According to the different weight content of PANI, these film samples were denoted as TiO₂, 2% PANI/TiO₂, 4% PANI/TiO₂, 6% PANI/TiO₂ and 8% PANI/TiO₂ respectively.

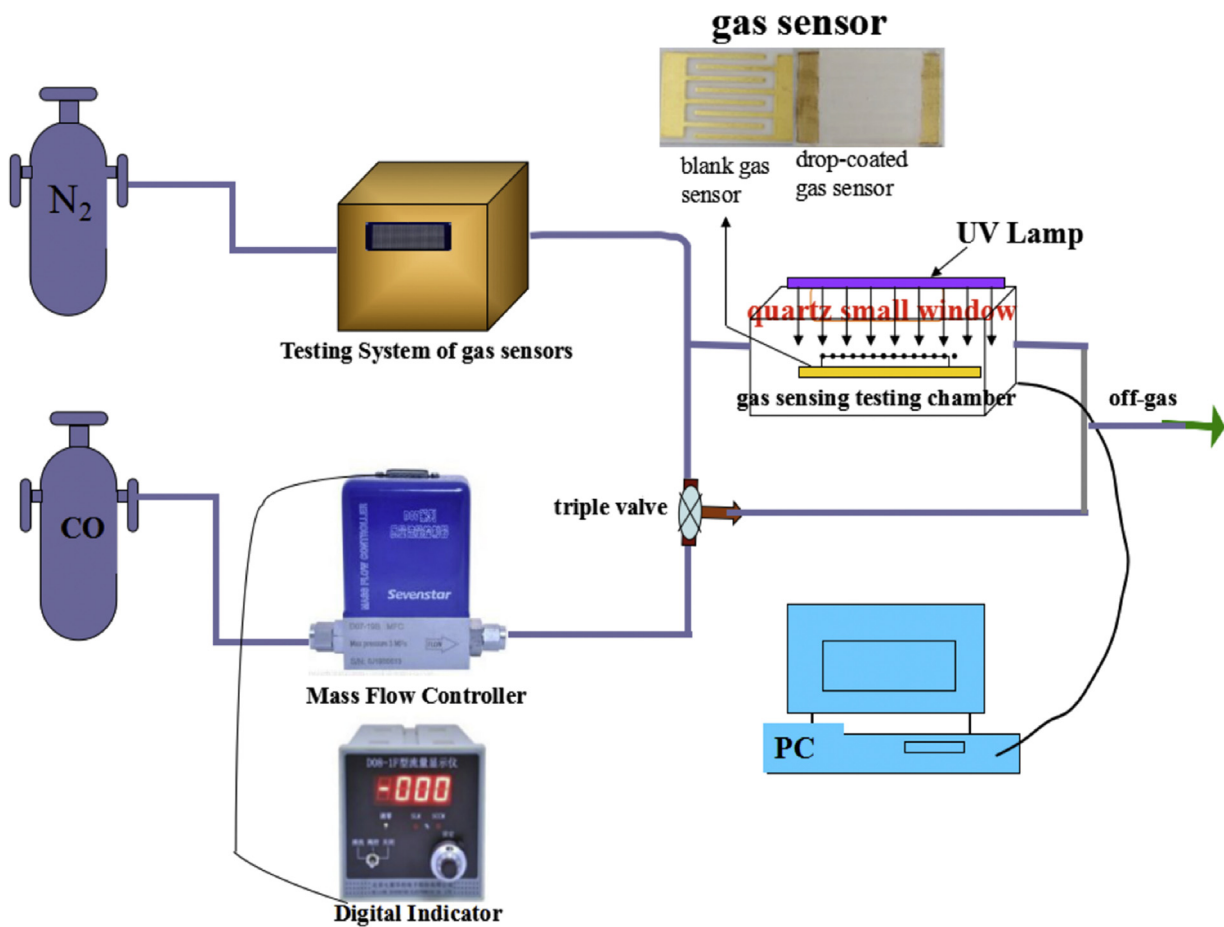
To further characterize the structure and surface properties of PANI/TiO₂ film, the PANI/TiO₂ films were peeled from the alumina substrates to obtain the respective PANI/TiO₂ powder samples.

2.3. Characteristics of PANI/TiO₂ samples

The X-ray diffraction (XRD) patterns of the samples were investigated on a Bruker D8 Advance X-ray diffractometer using Cu Kα radiation, where the diffracted X-ray intensities were recorded as a function of 2θ. The accelerating voltage and the applied current were 40 kV and 40 mA, respectively. UV-vis diffuse reflectance spectroscopy (UV-vis DRS) was recorded by means of a UV-vis spectrophotometer (Cary-500, Varian Co.), in which BaSO₄ was used as the background. Moreover, thermogravimetric analysis (TGA) was carried out on Netzsch STA 449 F3 Thermo analyzer with a heating rate of 10 °C min⁻¹ and a flowing air of 20 mL min⁻¹. The surface morphology of the prepared thickness films was performed by Scanning Electron Microscopy (SEM, the MIRA/TESCAN-FESEM scanning electron microscope). Apart from those, spectroscopic analysis of the samples was conducted on the Fourier transform infrared (FT-IR) spectroscopy (USA, Thermo Nicolet CO. Nexus IR) in the range 4000–500 cm⁻¹. The sampling method was a KBr pellet method.

2.4. Photoelectrochemical properties

The electrochemical properties of the sample were performed on an electrochemical analyzer by means of three-electrode configuration. The FTO conductive glass coated with material film acted as the working electrode, with a Pt wire as the counter-electrode and Ag/AgCl (in saturated KCl) electrode as a reference electrode. An Na₂SO₄ (0.02 M) aqueous solution was used as the electrolyte. The working electrodes were prepared by dip-coating method as following process: first, the FTO conductive glasses were washed in an ultrasonic bath with ethanol, deionized water repeatedly in sequence, then dried at 80 °C for 2 h 5 mg powder sample was added to 800 μL absolute DMF to make slurry and then the suspension was dispersed by ultrasonic for 3 h 20 μL slurry was then injected



Scheme 1. Schematic block diagram of the photo-assisted gas sensing testing device.

onto the conductive surface of a $2.5\text{ cm} \times 1.0\text{ cm}$ FTO glass electrode with the cell size of $5\text{ mm} \times 5\text{ mm}$. To obtain conductive working electrode, the non-conductive nail polish was brushed coating on the conductive surface of FTO glass. At last, the coated FTO glass electrode was dried at room temperature for 12 h.

2.5. Gas sensing performances

The gas sensing properties of film sensors was performed in a chamber shown in Scheme 1, which presented the whole procedure and the real gas chamber picture [29,34]. The chamber with a total volume of 100 mL was made of stainless steel. Four UV lamps with a wavelength centered at 365 nm (4 W , Philips TL/05) were used as the irradiation source and the total light intensity on the surface of sensing film was 7.3 mW cm^{-2} . The response of film sensor to the gas is described by the variation of its impedance. A high purity N_2 was introduced into the chamber as the background atmosphere, and CO (balance with the high purity He) as the probe gas. The total flow rate was kept at 250 mL min^{-1} . The mass flow meters were used to adjust different concentrations of the testing gas in the mixed gas. The resistance of the film sensor was measured by a JFO2E gas sensing test system (Kunming GuiYanJinFeng Tech. Corp. Ltd.) and the applied voltage was controlled at 8.5 V . In order to remove the water and the other gas adsorbates over the surface of gas sensor, the film sensor sample was maintained at 200°C for 1 h in a high purity N_2 before testing. Note that all the above experiments were carried out at room temperature. The relative CO sensitivity (S) of the sensor sample was defined as $S = R_0/R_{CO}$, where R_{CO} and R_0 were the impedance measured in the testing gas and in the background atmosphere, respectively.

2.6. Photocatalytic performances

The catalytic oxidation of CO over the obtained catalyst sample was conducted in a 50 mL quartz reaction tube. A 300 W Xe lamp with a 420 nm reflector was provided as UV light resource (the light intensity at $321\text{--}390\text{ nm}$ on the surface of catalyst sample was about 1.35 mW cm^{-2}). 0.5 g catalyst with a grain size of $0.2\text{--}0.3\text{ mm}$ was loaded on the bottom of batch. The reacted gases with 3.0 vol.\% CO , 3.0 vol.\% O_2 and a balance He were introduced into the batch with gas sample needle. After 1 h, the reacted gas was analyzed using an offline gas chromatograph system equipped with a thermal conductivity detector and a flame ionization detector (Agilent 4890D, Porapak R).

3. Results and discussion

3.1. Surface morphologies of PANI/TiO₂ film samples

The surface morphologies of gas sensor film and nanocomposite were characterized by SEM as shown in Fig. 1. It can be seen that the surface of pure TiO_2 sensor sample was an integrated thick film with a large of granular nanoparticles stacked together randomly (Fig. 1(a)). Moreover, a small amount of doping PANI into TiO_2 could hardly cause the change in surface morphology of gas sensor (seeing Fig. 1(a-e)), which could be also observed from the high-magnification SEM images of TiO_2 and 4%PANI/ TiO_2 (Fig. 1(f) vs. Fig. 1(g)). Moreover, the EDS elemental analysis results of 4%PANI/ TiO_2 confirmed that PANI was successfully doped into TiO_2 (seeing Fig. 1(h)).

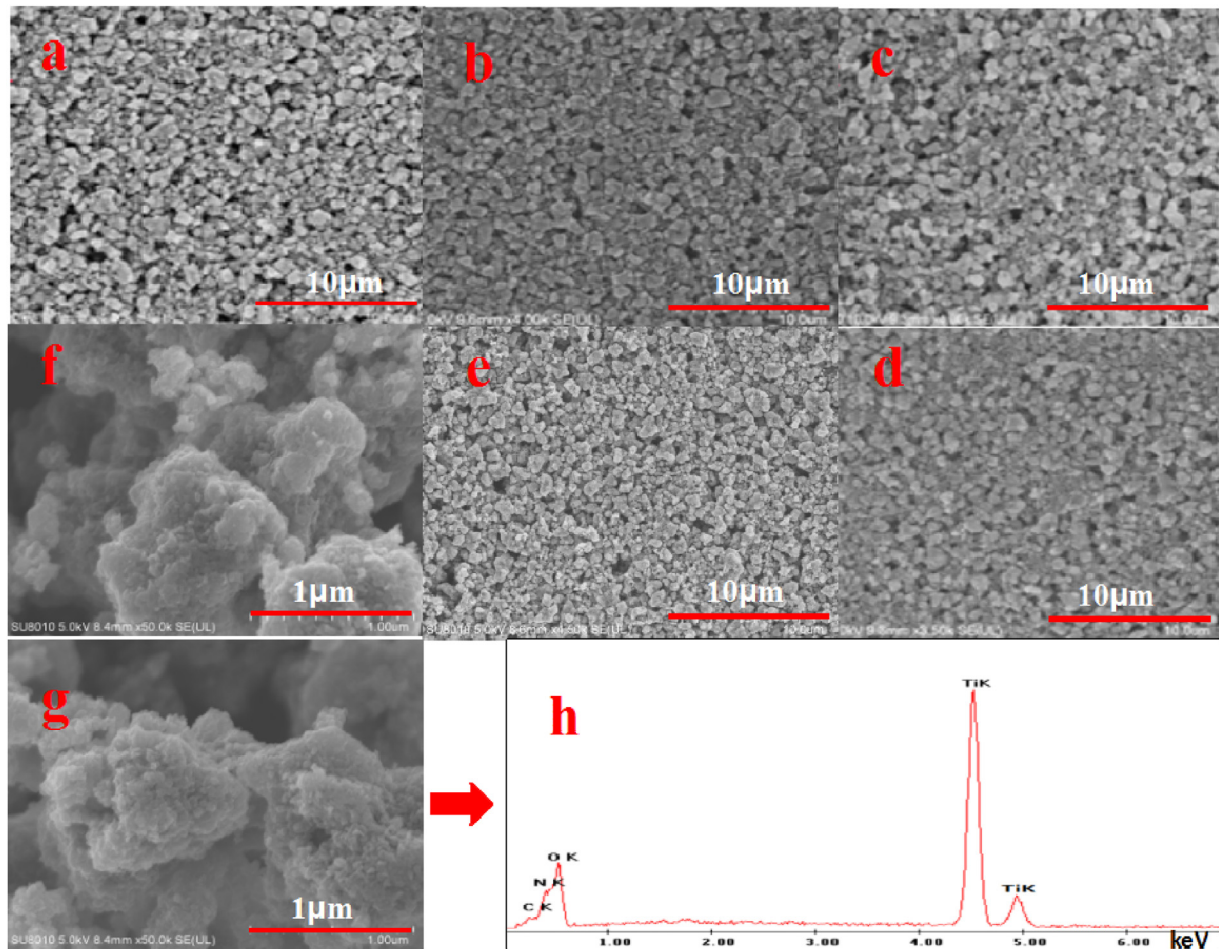


Fig. 1. SEM images of gas sensor surface of TiO₂ and the different PANI/TiO₂ samples: (a) pure TiO₂; (b) 2%PANI/TiO₂; (c) 4%PANI/TiO₂; (d) 6%PANI/TiO₂; (e) 8%PANI/TiO₂; (f) pure TiO₂ in a high-magnification; (g) 4%PANI/TiO₂ in a high-magnification and (h) Energy-dispersive X-ray spectroscopic (EDS) elemental analysis of 4%PANI/TiO₂ sample.

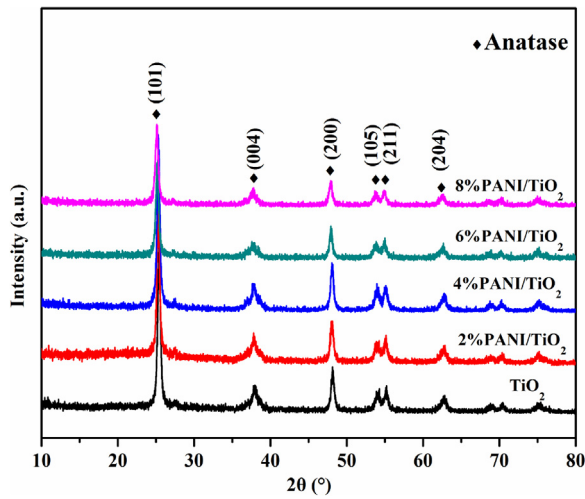


Fig. 2. The XRD spectra of TiO₂ and PANI/TiO₂ powder samples with different PANI contents prepared by an in-situ chemical oxidative polymerization.

3.2. The properties of PANI/TiO₂ powder samples

Fig. 2 shows the crystal structure of PANI/TiO₂ nanoparticles. The characteristic diffraction peaks at 2θ value of 25.37°, 48.06°, 54.0°, 55.1° and 62.8° can be assigned as (101), (200), (105), (211) and (204) crystal planes of anatase TiO₂ (JCPDS card 75–1537),

respectively. In comparison with pure TiO₂ sample, almost no significant changes were observed for the PANI/TiO₂ sample. Note that the PANI/TiO₂ samples did not exhibit the typical peak at 25° assigned to the XRD pattern of PANI [5]. This indicates that the process of introducing PANI into TiO₂ by in-situ polymerization method did not change the crystalline structure of anatase TiO₂. Of course, the main diffraction peak of PANI at 25° could be shielded by that of anatase TiO₂ at 25.37°.

Fig. 3 shows the UV-vis diffuse reflectance spectra (DRS) of different samples. Note that the spectrum of all samples exhibited a strong absorption band in the UV region (<380 nm), which mainly attributed to the intrinsic absorption of TiO₂. Owing to the pure PANI show an absorption in the visible region, the introduction of PANI into TiO₂ could extend the light absorption region into the visible light region. This light absorption of PANI could be attributed to the charge transfer-excitation like transition from the highest occupied molecular orbital (HOMO) to the lowest unoccupied molecular orbital (LUMO) i.e., the $\pi-\pi^*$ transition in the benzenoid and quinonoid units), which could promote the photocatalytic activity of TiO₂ in the visible light region [35,36].

To estimate thermal stability of PANI/TiO₂, thermogravimetric analysis (TG) of pure TiO₂, pure PANI and PANI/TiO₂ (4%PANI/TiO₂) were conducted in the temperature range of 0–1000 °C. As seen in Fig. 4, the PANI/TiO₂ is stable for TiO₂ below 800 °C which few weight loss. Note that thermal decomposition underwent a two-step weight loss pattern for PANI/TiO₂. During the first step process, the weight loss from 30 °C to 150 °C could be attributed to the desorption of moisture (physical adsorption H₂O) [37], while that

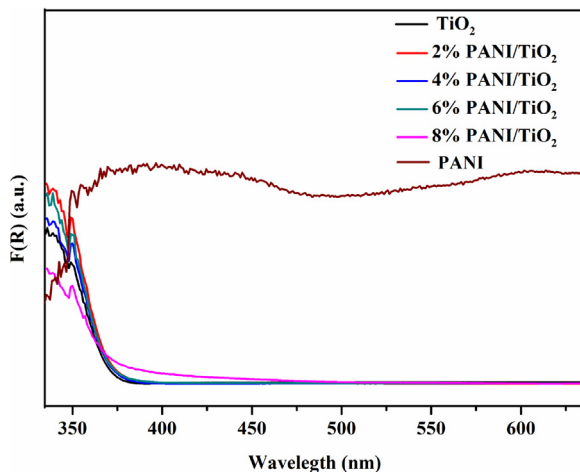


Fig. 3. UV-vis diffuse reflectance spectra (DRS) of TiO_2 , PANI and PANI/TiO_2 samples with different PANI contents.

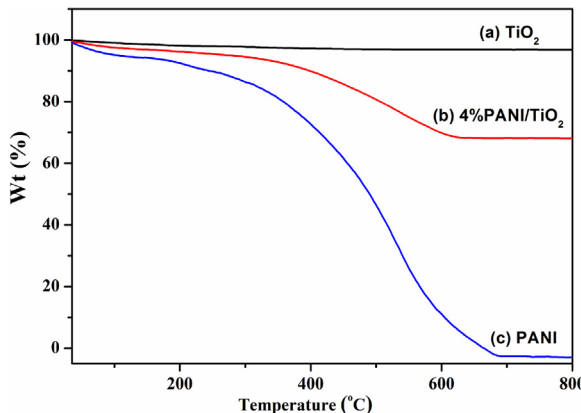


Fig. 4. TG curves of (a) TiO_2 , (b) 4%PANI/TiO₂ and (c) PANI powder samples performed in air atmosphere.

around 300 °C can be attributed to the removal of impurities and other oligomers. During the second step from 400 to 700 °C, the weight loss may be on account of the decomposition of PANI chains and pristine PANI backbone respectively [36]. With comparison to the pure PANI, the PANI/TiO₂ exhibited a similar thermal decomposition trend but with a higher decomposition temperature of PANI, indicating that the stability of PANI/TiO₂ mainly depend on PANI not TiO_2 . This result also showed that the PANI/TiO₂ film sensor would keep stable after calcining in air below 350 °C.

3.3. FT-IR spectra of TiO_2 , PANI and PANI/TiO_2 powder samples

Fig. 5 shows the FT-IR spectra of TiO_2 , PANI and PANI/TiO_2 (4%PANI/TiO₂) samples. The absorption peak at about 672 cm⁻¹ in TiO_2 and PANI/TiO_2 samples could be associated to Ti—O—Ti band, while the absorption peak at about 1633 cm⁻¹ in the two samples could be assigned to Ti—O stretching mode [38]. However, the peak at 1633 cm⁻¹ of PANI/TiO_2 was weaker than that of pure TiO_2 , indicating that doping PANI into TiO_2 could weaken the Ti—O stretching vibration. Note that PANI/TiO_2 exhibited the absorption bands in 1600–1000 cm⁻¹ similar to the pure PANI sample. Here, the peaks at 1586 cm⁻¹, 1504 cm⁻¹ and 1301 cm⁻¹ could be ascribed to the C=N stretching vibration for the quinoid ring, the C—N stretching vibration of quinoid ring and the C—N stretching vibration of benzenoid ring [39–41], respectively. In addition, the absorption peak at 1150 cm⁻¹ could be assigned to the N—H stretching vibration, while that at 1140 cm⁻¹ could be attributed to the anin-plan bend-

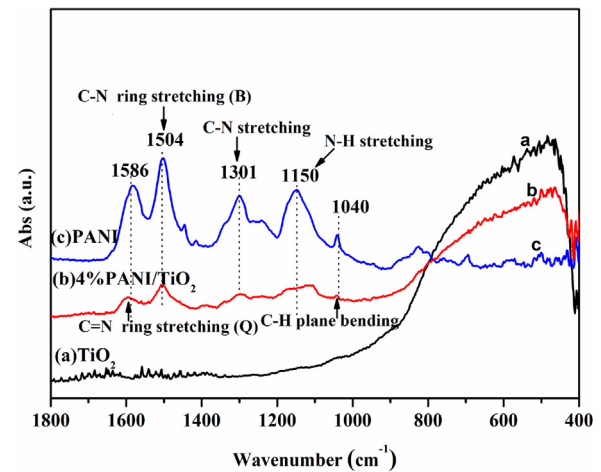


Fig. 5. FT-IR patterns of (a) TiO_2 , (b) 4%PANI/TiO₂ and (c) PANI powder samples.

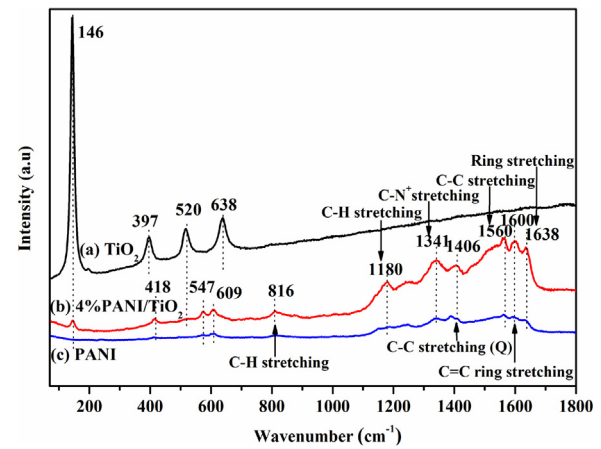


Fig. 6. Raman patterns of (a) TiO_2 , (b) 4%PANI/TiO₂ and (c) PANI powder samples.

ing vibration of C—H [42–45]. These characteristic bonds confirmed that PANI existed in PANI/TiO_2 in the state of an emeraldine salt phase. Moreover, the decrease in the absorption intensities of PANI (PANI/TiO_2 vs. PANI) also means that there may be also exhibit an interaction between PANI chains and TiO_2 nanoparticles ulteriorly.

3.4. Raman spectra of samples

Fig. 6 shows the Raman spectra of TiO_2 , PANI and PANI/TiO_2 samples. The pure TiO_2 sample showed four characteristic peaks at 147, 397, 520 and 638 cm⁻¹, which were assigned as the Eg phonon, B1g, A1g and Eg modes of the anatase structure [46], respectively. However, the introduction of PANI into TiO_2 would weaken these characteristic peaks of TiO_2 , which only the peak at 147 cm⁻¹ of TiO_2 could be observed, while other three peaks at 397, 520 and 638 cm⁻¹ of TiO_2 did not appear in PANI/TiO_2 sample. This indicates that the presence of PANI could weaken the polarizability of TiO_2 lattice field. On the contrary, the presence of TiO_2 enhanced the characteristic peaks of PANI, i.e., PANI/TiO_2 exhibited the stronger absorption peaks assigned to PANI than PANI sample. As seen in Fig. 6, all the peaks at 1180 cm⁻¹ (C—H bending vibration of the benzenoid or quinoid rings), 1341 cm⁻¹ (related to C—N⁺ stretching vibration [37]), 1406 (1560) cm⁻¹ (C—C stretching vibration), 1600 cm⁻¹ (C=C stretching vibration of the benzenoid ring), and 1638 cm⁻¹ (benzenoid or quinonoid ring bending vibration) of PANI [47] were enhanced by the introduction of TiO_2 . In addition, the peaks at 418, 547, 609 and 816 cm⁻¹, related to the C—H deforma-

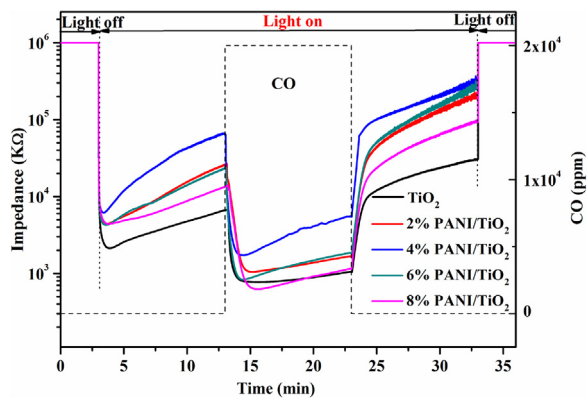


Fig. 7. Gas sensitivities to CO over TiO_2 and PANI/TiO_2 samples with different PANI contents under UV irradiation at room temperature.

Table 1
The photo-assisted gas sensitivity to CO of TiO_2 , PANI and PANI/TiO_2 samples.

Sample	Impedance (R)		$S = R_0/R_{CO}$
	R_0 (k Ω)	R_{CO} (k Ω)	
TiO_2	6665	771	8.65
2%PANI/TiO ₂	26497	1042	25.43
4%PANI/TiO ₂	68422	1680	40.73
6%PANI/TiO ₂	23661	836	28.3
8%PANI/TiO ₂	13674	628	21.77
^a PANI	10^6	10^6	1.00

^a For the PANI sensor sample, the impedances of both R_0 and R_{CO} were higher than the detection limit of the device (10^6 k Ω), resulting in no apparent response ($S = 1$).

tion of PANI [47], also increased obviously in PANI/TiO_2 . This Raman testing result further indicates that a strong interaction existed between PANI and TiO_2 in PANI/TiO_2 .

3.5. Gas sensing responses of PANI/TiO_2 under UV irradiation

Fig. 7 shows the gas sensing performances of TiO_2 and PANI/TiO_2 sensor samples to CO in N_2 atmosphere at room temperature under UV irradiation. As can be seen, the impedance of all sensors decreases rapidly with the introduction of the UV light in the high purity N_2 atmosphere, but increase gradually again with the increase of irradiation time, which was coincide with our previous report [32]. Apparently, UV light could excite TiO_2 to produce the photo-generated electrons, resulting in the increase in the surface electron density of nanocomposites. However, PANI/TiO_2 samples showed a higher impedance than pure TiO_2 sample, indicating that the introduction of PANI maybe suppressed the generation of photo-induced electrons or its transfer.

With the introduction of CO, the impedance of all samples decreased rapidly, indicating that CO as electron offer can provide the electrons to materials surface, resulting in the increase in the surface electron density of materials. Although the impedance increased slowly with the increase of time, it was still far lower than that prior to the introduction of CO. As CO stream is cut off, the surface impedance increased again, and finally returned to the detection limit with the removing UV light. Further comparing the gas sensitivity value (seen in **Table 1**), it can be seen that all PANI/TiO_2 sample exhibited a higher value of CO gas sensitivity than the pure TiO_2 , which the sensitivity value of 4% PANI/TiO_2 gas sensor was about 40.73, far higher than the pure TiO_2 and other PANI/TiO_2 samples. This result showed that introducing PANI into TiO_2 could enhance the photo-assisted gas sensitivity to CO, although it weakened the photo-assisted conductivity of film sensor sample at N_2 atmosphere. This also suggests there maybe exist

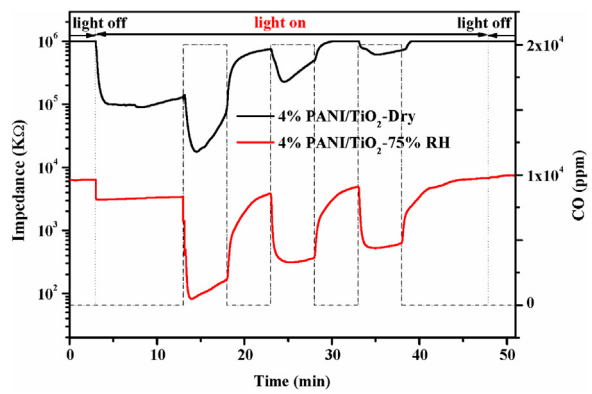


Fig. 8. Gas sensitivities to CO over 4%PANI/TiO₂ sample in a dry (the same atmosphere as that in **Fig. 7**) and a humidity (75% RH) N_2 atmosphere under UV irradiation at room temperature in three cycles, respectively.

a synergistic effect to photo-assisted gas sensing response to CO between the PANI and TiO_2 nanoparticles.

Note that the CO gas sensitivities of all PANI/TiO_2 samples under UV light decreased along with time in **Fig. 7**. This may be caused by the consumption of surface chemisorbed water (the chemisorbed CO reacting with the surface hydroxyls at TiO_2 [32]) on samples during the testing process. Our previous work has ever found that the presence of H_2O could promote the gas sensitivity performance of TiO_2 sensor to ethylene [34]. To further confirm the viewpoint, the repeatability about the CO gas sensitivity of 4%PANI/TiO₂ sample was compared in a dry and a humidity N_2 atmosphere, respectively. As seen in **Fig. 8**, in the dry N_2 atmosphere (no extra water introduced into the testing system, just like that in **Fig. 7**), the impedance of sensor sample increased along with time in the first cycle and further increased in the second and third cycle, indicating that a weak stability and repeatability about the photo-assisted CO gas sensitivity. However, in the humidity N_2 atmosphere (the background N_2 gas passing through a saturated NaCl solution, here the relative humidity (RH) in the atmosphere kept at 75% [34]), although the CO gas sensitivity in the second or the third cycle was weaker than that in the first cycle, the sensitivity value was almost stable, exhibiting a much better stability and repeatability than that in the dry N_2 atmosphere. This indicates that the introduction of water actually enhanced the CO gas sensitivity of PANI/TiO_2 sample. A more detailed explanation will be discussed in the following section.

3.6. Photocurrents

Considering that the photo-generated electron transfer behavior of sensor sample would play a role on its photo-assisted gas sensing performance, the photoelectrochemical measurements of different samples were tested. **Fig. 9** shows the photocurrent-time curves of pure TiO_2 and PANI/TiO_2 samples with different content of PANI. The photocurrent values of all samples increased rapidly with the introduction of UV light, and decreased rapidly as soon as the lamp is turned off, indicating that the photo-generated electrons could transfer from TiO_2 to the FTO substrates to produce photocurrent under UV irradiation [36]. Although the initial photocurrent values of 2%PANI/TiO₂ and 6%PANI/TiO₂ were superior to that of TiO_2 under UV irradiation, they decreased rapidly in the subsequent recycle testing, even lower than that of TiO_2 . For 8%PANI/TiO₂, it exhibited a lower photocurrent value than TiO_2 during the testing cycles. This result is accordance with the result of impedance of samples under UV irradiation in N_2 atmosphere in **Fig. 6**, i.e., the photo-assisted conductivities of PANI/TiO_2 samples were lower than that of TiO_2 . Note that the 4%PANI/TiO₂ owned a higher photocurrent value than TiO_2 , even after several recycles,

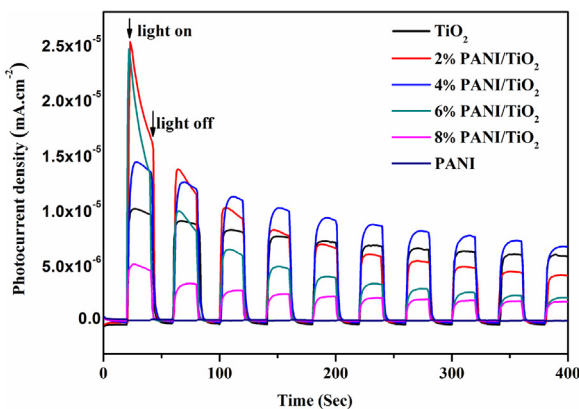


Fig. 9. Photocurrent responses of TiO_2 , PANI and PANI/ TiO_2 samples under UV irradiation.

which was inconsistent with the result in Fig. 6. This indicated that the photo-assisted conductivities of TiO_2 or PANI/ TiO_2 samples in Na_2SO_4 solution were different from those in gas atmosphere. However, the highest photocurrent value of 4%PANI/ TiO_2 in all samples seems to be consistent with the highest gas sensitivity to CO of 4%PANI/ TiO_2 . This result also indicated that adding PANI into TiO_2 could lead to the change in electron generation, separation and transfer behaviors.

As for the observed decreases of photocurrents along with time over PANI/ TiO_2 samples in Fig. 9, it could be attributed to the change in surface structure of PANI and TiO_2 during the testing process. Since the photocurrent test was conducted in aqueous phase, the H_2O molecules maybe changed the surface states of TiO_2 and PANI and then made an influence on the electron transfer at the interface of PANI and TiO_2 , resulting in the decrease of photocurrent along with time. This instability of photocurrent also occurred on the pure TiO_2 sample due to the change in surface state of TiO_2 induced by H_2O molecules. However, the photocurrent value of TiO_2 sample during the testing cycles was more stable than that of PANI/ TiO_2 sample due to the absence of electron transfer at the interface of PANI and TiO_2 .

3.7. Electron transfer between PANI and TiO_2 characterized by XPS analysis

To further explore the electron transfer between PANI and TiO_2 , the chemical state of elements in PANI, TiO_2 and 4%PANI/ TiO_2 samples were compared by a XPS analysis. Fig. 10(a-d) shows the XPS spectra of PANI, TiO_2 and PANI/ TiO_2 nanocomposites. As seen in Fig. 10(a), the C1s XPS spectrum of PANI/ TiO_2 could be deconvoluted into three species, the peaks at 284.20 eV, 284.80 eV and 285.75 eV could be related to C=C or C-H bonds, C-N or C=N bonds and C=N⁺ or C=C=N⁺ bonds, respectively [48,49]. The positive shift in BE of C-C/C=C, C-N/C=N and C-N⁺/C=C=N⁺ for PANI/ TiO_2 from 284.20, 284.80 and 285.75–284.45, 284.85 and 285.85 eV in comparison with PANI, respectively, indicating that the interaction would occur between TiO_2 and PANI (maybe forming the structure of Ti—O—N—C [50] and Ti—O—C [50,51]). In addition, the peak at 287.80 eV was associated to the functional group C=O/C—O which could arise from the formation of benzoquinone and hydroquinone as the excessive oxidation products of polyaniline.

In addition, the O1s XPS spectrum of TiO_2 could be resolved into two peaks in Fig. 10(b), i.e., the lower peak at 529.10 eV for O (1s) assigned to the typical the lattice oxygen oxide of Ti—O and the higher peak at 530.70 eV ascribed to the surface hydroxyl (Ti—O—H) of TiO_2 , respectively [52]. Compared to that of TiO_2 , the BE values of both two oxygen species of PANI/ TiO_2 presented a positive shift (from 529.10 and 530.45 eV for the lattice oxygen and from 530.70

to 532.30 eV for the surface hydroxyl groups, respectively). This indicated that the surface hydroxyl groups or the lattice oxygen of the TiO_2 was also probably participated into the bonding reaction with the imine ($=\text{N}=$) or amine ($-\text{NH}-$) groups of PANI by the formation of copious hydrogen bond network ($\text{TiO}_2-\text{O}-\text{HN}-\text{PANI}$) during the assembly process of the polymerization of aniline [33]. Moreover, this decrease in the surface electron density of O species means that the electrons would transfer from TiO_2 to PANI at the interface of PANI and TiO_2 . Moreover, the BE values of Ti 2p3/2 (459.30 eV) or Ti 2p1/2 (465.10 eV) of PANI/ TiO_2 exhibited a positive shift of 0.6 eV compared to those of Ti2p3/2 (458.70 eV) or Ti2p1/2 (464.50 eV) of TiO_2 (Fig. 10(c)), also indicating that the introduction of PANI reduces the surface electron density of TiO_2 .

Fig. 10(d) shows the N1s XPS spectrum of PANI and PANI/ TiO_2 samples. For PANI sample, the N1s peak could be resolved into three peaks at 399.14, 400.05 and 401.35 eV, assigned to the benzenoid diamine ($-\text{NH}-$), the quinoid remain-diimine species ($=\text{N}=$) and the protonated amine species ($-\text{N}^+$), respectively [33,53,54]. As compared to that of PANI, all the N1s BE value of three N species in PANI/ TiO_2 made a negative shift (from 399.14, 400.05 and 401.35 eV to 398.50, 399.45 and 400.20 eV, respectively), also indicating that the electrons would transfer from TiO_2 to PANI over PANI/ TiO_2 . Moreover, a new N1s peak at 402.25 eV could be observed over PANI/ TiO_2 , which could be attributed to the protonated imine species ($=\text{N}^+$) caused by the surface hydroxyl groups of TiO_2 with an interchain H-bonding. This protonation behavior of PANI would bring about the electronic defects in the polymer chain such as polarons or bipolarons [55]. In fact, it is the protonation behavior of the $-\text{N}=$ or the oxidation of the $-\text{NH}-$ to act as a better electron transfer and highly conductive state [56].

This above XPS result indicated that there existed an interaction between PANI and TiO_2 by forming the hydrogen bonding between surface hydroxyl of TiO_2 , and the protonated N in PANI chains [50]. Moreover, both the increase in surface electron density of N atoms of PANI and the decrease in that of TiO_2 indicate that this interaction would lead to the electron transfer from TiO_2 to PANI. Note that the positive shift in C1s of PANI/ TiO_2 as compared to that of PANI means a decrease in the surface electron density of C atom of PANI in the presence of TiO_2 . This also shows that the C atoms maybe offer electrons to TiO_2 by forming the structure of Ti—O—C. Overall, the electrons would transfer from TiO_2 to PANI at the interface of TiO_2 and PANI.

3.8. Proposed process of photo-assisted conductivity and gas sensitivity of PANI/ TiO_2

Based on the above XPS analysis result, the interaction of TiO_2 and PANI can be proposed in Fig. 11. Here, electrons would transfer from TiO_2 to PANI by the hydrogen bonds ($\text{TiO}_2\cdots\text{H}\cdots\text{N}-\text{PANI}$), and then transport in PANI by the polaron lattice in PANI chain and the p- π delocalized conjugated structure (formed by the p orbital of N atom with the π delocalized conjugated benzenoid or quinonoid unit) [26]. However, it is essential for an electron transport in PANI backbone to create an electron hopping from a chain to another, i.e., the electron transfer have to overcome a potential barrier between chains.

When PANI/ TiO_2 was exposed to CO, CO molecule would be adsorbed at the protonated N atom to form a bridge like as carbonyl group in two adjacent chains. This carbonyl group may be benefit to the electron from CO to PANI, and then to TiO_2 by the new formed hydrogen bonds ($\text{N}\cdots\text{H}\cdots\text{O}$) (the interaction of the adjacent amine nitrogen of PANI chain and TiO_2). Of course, the CO may also directly be adsorbed at TiO_2 sites, which offer electrons to TiO_2 . Obviously, CO molecules are more easily adsorbed at PANI/ TiO_2 than TiO_2 .

In fact, PANI can be also regarded as a narrow band gap semi-conductor from HOMO to LUMO (corresponding to the $\pi-\pi^*$

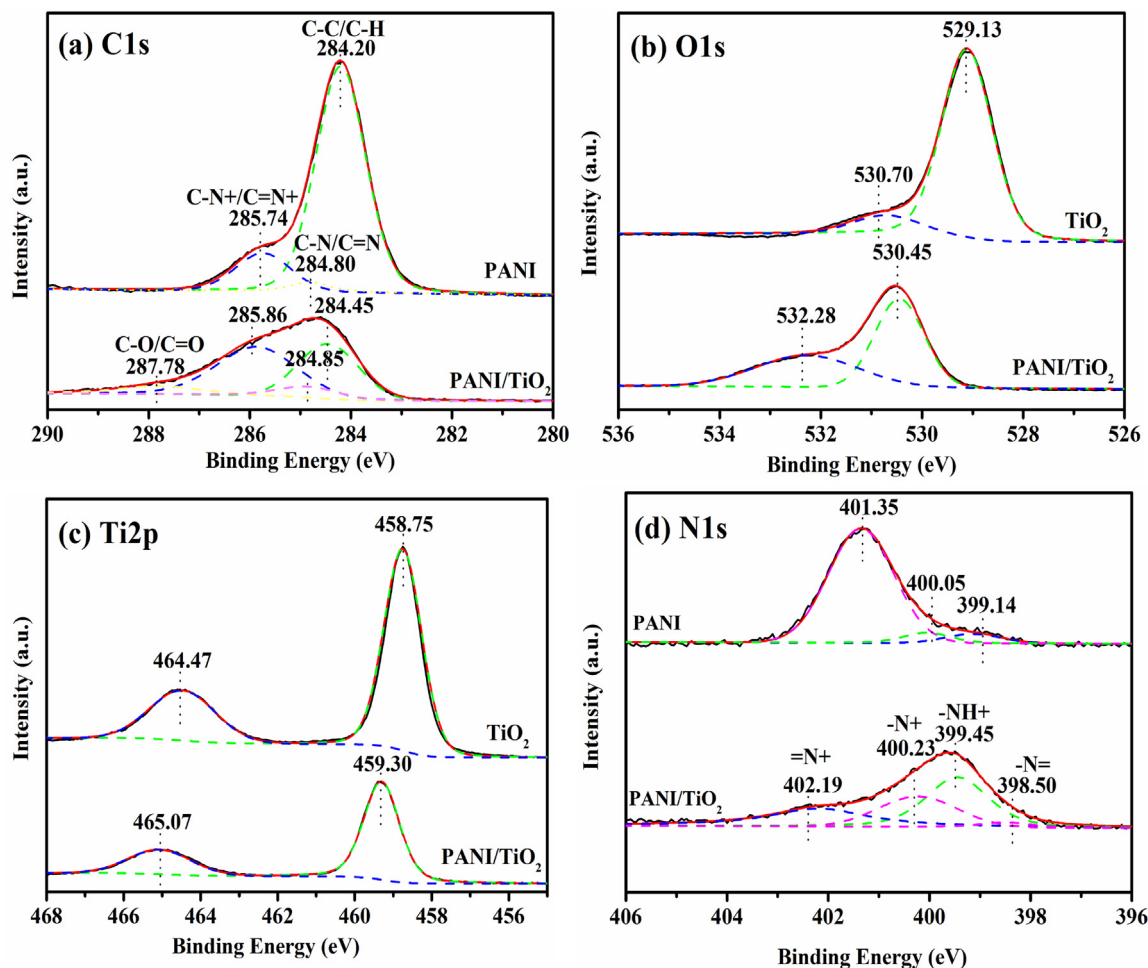
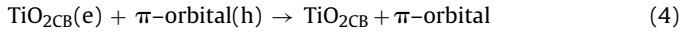
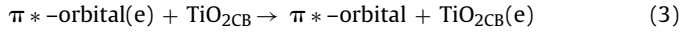
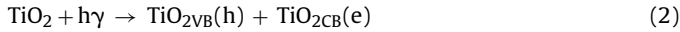
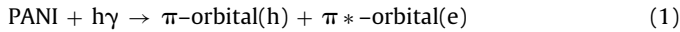


Fig. 10. XPS spectra of PANI, TiO₂ and PANI/TiO₂ samples: (a) C1s spectra of PANI and PANI/TiO₂; (b) O1s spectra of TiO₂ and PANI/TiO₂; (c) Ti2p spectra of TiO₂ and PANI/TiO₂; (d) N1s spectra of PANI and PANI/TiO₂.

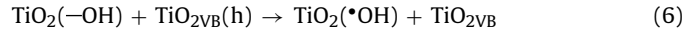
transition in the benzenoid and quinonoid units). According to our previous report [57], PANI owned a higher LUMO and HOMO level than the conductive band and valence band of TiO₂, respectively. Based on the energy levels of TiO₂ and PANI, the carrier transport process between PANI and TiO₂ under UV irradiation could be proposed as follows (also seeing Fig. 12(a)):



During the above processes, both PANI and TiO₂ could be activated into the excited state under UV irradiation (Eqs. (1) and (2)). Although PANI accepted electrons from TiO₂ without UV irradiation based on the above XPS result, the excited electrons in π^* -orbital (LUMO) were enabled to overcome the Schottky barrier at the interface between PANI and TiO₂, and then transfer into the CB of TiO₂ (Eq. (3)). Meanwhile, the excited-state electrons in the CB of TiO₂ could transfer into the π -orbital (HOMO) of PANI (Eq. (4)). Obviously, the photo-induced states under UV irradiation (Eqs. (1)–(3)) could form a channel for electron hopping from the chains of PANI to TiO₂ grain at the interface of PANI/TiO₂ [58]. However, the electron transfer behavior from TiO₂ to PANI (Eq. (4)) seemed to accelerate the recombination of electrons and holes, resulting in decrease of electrons from PANI/TiO₂ to the conducting Au sub-

strate. This may be one possible reason that PANI/TiO₂ exhibited a lower conductivity than TiO₂ in N₂ atmosphere.

As for the photo-generated holes in the VB of TiO₂ ($\text{TiO}_{2\text{VB}}$ (h) in Eq. (2)), some may be recombined with the photo-generated the photo-generated electrons ($\text{TiO}_{2\text{CB}}$ (e)), another holes may be captured by the surface hydroxyls at TiO₂ ($\text{TiO}_2(\text{--OH})$) to form the surface hydroxyl radicals ($\text{TiO}_2(\cdot\text{OH})$), resulting in that the more photo-generated free electrons could transfer into the Au substrate to form the current under a bias voltage. This may be one reason that the introduction of water could enhance the conductivity of PANI/TiO₂ sensor sample in N₂ atmosphere (seeing Fig. 8, here without CO). The two above processes could also occur on the pure TiO₂ sensor sample, which could be described as follows:



With the introduction of CO into the testing system under UV irradiation, CO could be adsorbed at both TiO₂ and PANI surface accompanied by providing electrons into PANI/TiO₂. On the one hand, the CO molecules adsorbed at TiO₂ surface would react with the surface hydroxyls (or hydroxyl radicals) [59], resulting in the proceeding of Eq. (6) (i.e., more holes in the VB of TiO₂ could be captured) and then the formation of more free electrons in the CB of TiO₂. Of course, the adsorbed CO at TiO₂ could also directly donate electrons to combine the holes in the VB of TiO₂. On the other hand, the CO molecules adsorbed at PANI surface (chemisorbed at the protonated N sites of PANI) could donate electrons to com-

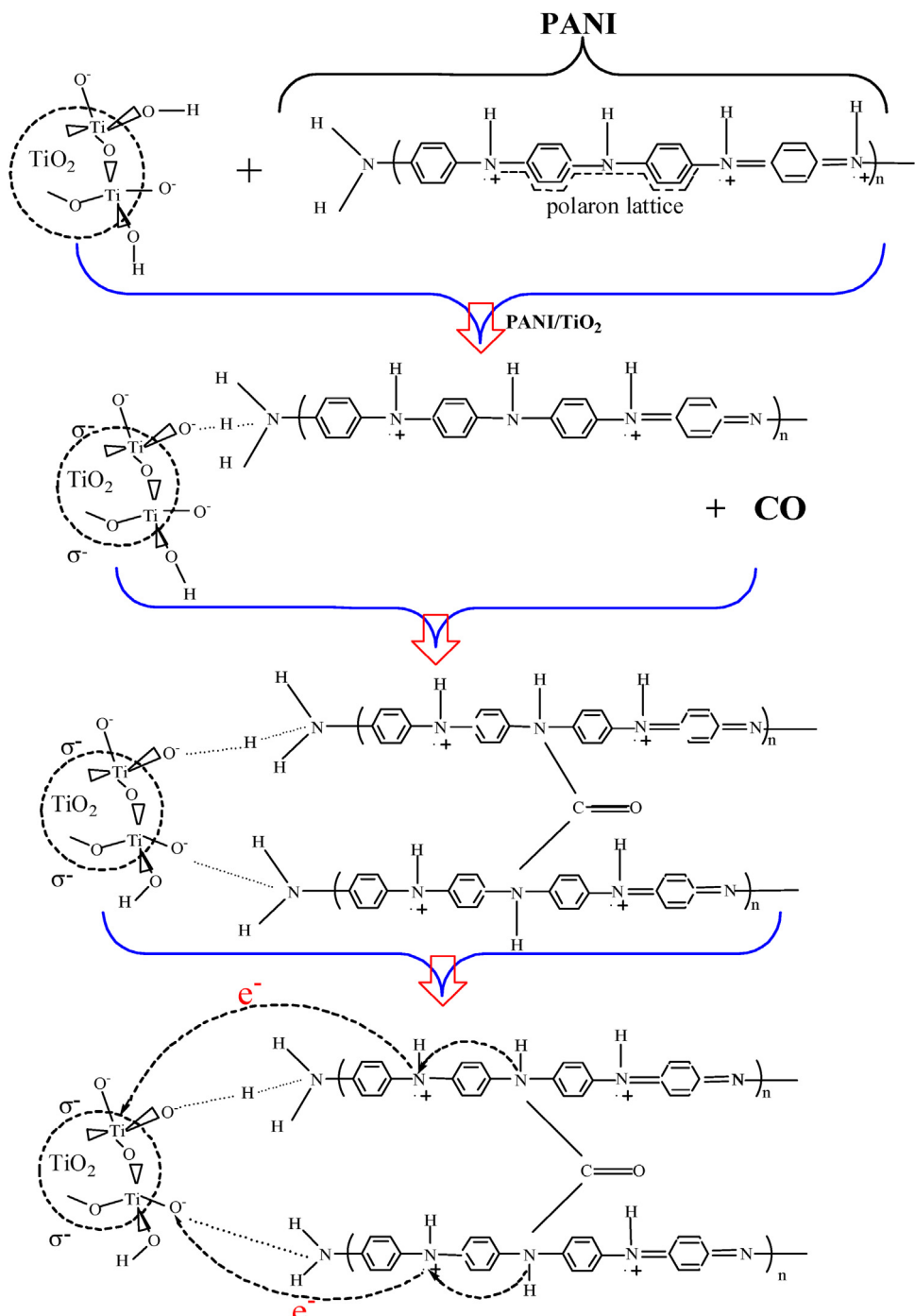
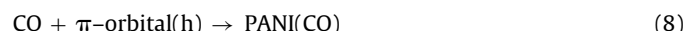


Fig. 11. The proposed interaction behavior between PANI and TiO₂ and the possible process of adsorbing CO at PANI/TiO₂ surface without UV light.

bine with the holes in the HOMO of PANI, resulting in the more free electrons in the LUMO of PANI being transferred to the CB of TiO₂ (these free electrons could transfer into the Au substrate to form the current). Here, the adsorbed CO at PANI maybe also further react with the hydroxyl radicals at TiO₂ surface just like that the adsorbed CO at TiO₂. As compared to that of TiO₂ sensor, the extra CO molecules chemisorbed at PANI would offer more electrons to the PANI/TiO₂, resulting in the stronger response to CO over PANI/TiO₂. This process could be described as follows (also seeing Fig. 12(b)):



However, the above process in Eq. (9) was an irreversible chemical reaction, which would cause the consumption of surface hydroxyls and then the decrease in CO gas sensitivity of PANI/TiO₂ with prolonging time under UV irradiation (seeing the curve of dry atmosphere in Fig. 8). Therefore, the introduction of water into PANI/TiO₂ could keep its stability of CO gas sensitivity (seeing the curve of 75% RH in Fig. 8).

Note that the pure PANI could not exhibit an apparent response to CO under UV irradiation, indicating that TiO₂ would be mainly responsible for the gas sensing response to CO over PANI/TiO₂.

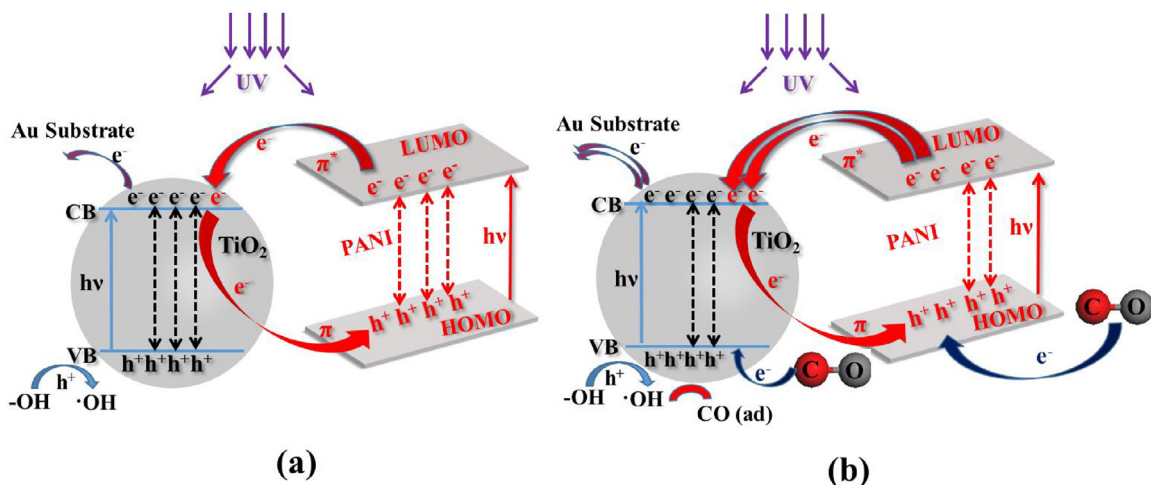


Fig. 12. The proposed mechanism of photo-assisted gas sensitivity to CO for PANI/TiO₂ at room temperature under UV irradiation: (a) No CO (electrons transferring from TiO₂ to PANI) and (b) adding CO (CO denoting electrons to both TiO₂ and PANI). In addition, the adsorbed CO at TiO₂ and PANI could further react with the hydroxyl radicals at TiO₂ surface formed by surface hydroxyls.

Table 2

The correlation between CO oxidation and CO sensitivity over TiO₂ and PANI/TiO₂ under UV irradiation.

Samples	CO oxidation (Increase in CO ₂ content, ppm)	CO sensitivity (S = R ₀ /R _{CO})	Characteristic
TiO ₂	4320	8.65	A weak CO sensitivity corresponding to the less CO oxidation
4%PANI/TiO ₂	13850	40.73	A strong CO sensitivity corresponding to the more CO oxidation

Therefore, the more content of PANI in PANI/TiO₂ maybe lead to the decrease of the UV photo-assisted gas sensitivity. As can be seen, it was the comment effect of both the extra CO adsorption at the protonated N sites of PANI and the electron transfer between PANI and TiO₂ to be responsible for the enhanced CO gas sensitivity of PANI/TiO₂ sample under UV irradiation.

3.9. Photocatalytic performances of oxidizing CO over TiO₂ and PANI/TiO₂

To further investigate the relation among the photo-assisted conductivity, the photo-assisted gas sensing and the photocatalytic performances, the photocatalytic activities of oxidizing CO into CO₂ over the pure TiO₂ and 4% PANI/TiO₂ samples have been evaluated by an intermittent device, respectively. It is found that the 4% PANI/TiO₂ sample could produce more CO₂ than the pure TiO₂ sample under UV irradiation for 1 h (13850 ppm vs. 4320 ppm), indicating that the former exhibited a higher photocatalytic activity than the latter, in accordance with the compared result of CO sensitivities of two samples (i.e., 4% PANI/TiO₂ sample exhibited a higher CO sensitivity than the pure TiO₂ sample in Table 1). As can be seen, the enhanced response to CO induced by adding PANI could be favor of the oxidation of CO over PANI/TiO₂ under UV irradiation. In fact, the photo-assisted response to CO of sample could be regarded as the CO chemisorption process or the CO pre-oxidized process [32]. As compared to that of TiO₂ sample, the higher CO sensitivity of PANI/TiO₂ means that the adsorbed CO could denote more electrons to PANI/TiO₂ (i.e., the more CO could be pre-oxidized) under UV irradiation, resulting in the more CO being oxidized. This correlation between CO sensitivity and its oxidation behavior could be concluded in Table 2.

This above result shows that the photocatalytic activity of oxidizing CO over the TiO₂-based semiconductor maybe somewhat depended on the chemisorption behavior of CO, of which could also be evaluated by the gas sensitivity. That is to say, the photo-assisted gas sensitivity of semiconductor catalyst could be regarded as an indirect index of evaluating the photocatalytic activity to some extent.

4. Conclusions

The photo responsive properties of PANI/TiO₂ samples and their sensing responses to CO under UV irradiation were performed at room temperature. Doping PANI into TiO₂ would weaken the photo-induced conductivity of TiO₂ at N₂ atmosphere, but enhance the photo-assisted sensing response to CO under UV irradiation. The characteristic properties of PANI/TiO₂ showed there maybe exist an interaction between PANI and TiO₂ by forming a hydrogen bond and a protonated N site, resulting in electrons would transfer from TiO₂ to PANI at the interface of PANI and TiO₂ without UV light. Under UV irradiation, the excited electrons in π*-orbital of PANI were enabled to overcome the Schottky barrier at the interface between PANI and TiO₂, and then transfer into the CB of TiO₂. Meanwhile, the electrons in CB of TiO₂ maybe also transfer back into PANI and then recombine with holes in PANI, resulting in a lower photo-induced conductivity of PANI/TiO₂ than that of TiO₂ at N₂ atmosphere. However, the promoted CO adsorption at the protonated N sites of PANI would offer more electrons to PANI and then TiO₂, resulting in a stronger gas sensitivity to CO over PANI/TiO₂. Moreover, the introduction of H₂O could promote the CO gas sensitivity of PANI/TiO₂ due to the formation of surface hydroxyls and the subsequent hydroxyl radicals. Furthermore, this enhanced CO sensitivity would be favor of CO oxidation under UV irradiation. This result shows that the photocatalytic activity of oxidizing CO over the TiO₂-based semiconductor maybe somewhat depended on the photo-assisted sensitivity to CO.

Acknowledgments

This work was financially supported by the National Natural Science Foundation of China (no. 21273037), the National Basic Research Program of China (973 Program, no. 2014CB239303), the National Key Technologies R&D Program of China (no. 2014BAC13B03) and the Science & Technology Plan Project of Fujian Province (no.2014Y2003).

References

- [1] B. Renganathan, G. Gobi, D. Sastikumar, R. Srinivasan, A.C. Bose, Optical fibercoated with nanocrystalline tin oxide for ammonia vapour sensing, *Sens. Lett.* 8 (2010) 292–296.
- [2] X. He, X.J. Zhao, B.S. Liu, The synthesis and kinetic growth of anisotropic silver particles loaded on TiO₂ surface by photoelectrochemical reduction method, *Appl. Surf. Sci.* 254 (2008) 1705–1709.
- [3] J.J. Hassan, M.A. Mahdi, C.W. Chin, H. Abu-Hassan, Z. Hassan, A high-sensitivity room-temperature hydrogen gas sensor based on oblique and vertical ZnO nanorod arrays, *Sens. Actuators B: Chem.* 176 (2013) 360–367.
- [4] V. Srivastava, K. Jain, Highly sensitive NH₃ sensor using Pt catalyzed silica coating over WO₃ thick films, *Sens. Actuators B: Chem.* 133 (2008) 46–52.
- [5] R. Bene, I.V. Perczel, F. ReÄti, F.A. Meyer, M. Fleisher, H. Meixner, Chemical reactions in the detection of acetone and NO by a CeO₂ thin film, *Sens. Actuators B: Chem.* 71 (2000) 36–41.
- [6] G.Z. Cao, *Nanostructures and Nanomaterials: Synthesis, Properties and Applications*, Imperial College Press, London, 2004.
- [7] H.R. Tantawy, D.E. Aston, J.R. Smith, J.L. Young, Comparison of electromagnetic shielding with polyaniline nanopowders produced in solvent-limited conditions, *ACS Appl. Mater. Interfaces* 5 (2013) 4648–4658.
- [8] M. Matsuguchi, A. Okamoto, Y. Sakai, Effect of humidity on NH₃ gas sensitivity of polyaniline blend films, *Sens. Actuators B: Chem.* 94 (2003) 46–52.
- [9] H.L. Tai, Y.D. Jiang, G.Z. Xie, J.S. Yu, X. Chen, Fabrication and gas sensitivity of polyaniline–titanium dioxide nanocomposite thin film, *Sens. Actuators B: Chem.* 125 (2007) 644–650.
- [10] D.W. Hatchett, Mira Josowicz, Composites of intrinsically Conducting Polymers as sensing nanomaterials, *Chem. Rev.* 108 (2008) 746–769.
- [11] J. Li, H.Q. Xie, Y. Li, Fabrication of gold nano-particles/polypyrrole composite-modified electrode for sensitive hydroxylamine sensor design, *J. Solid State Electrochem.* 16 (2012) 795–802.
- [12] M. Joubert, M. Bouhadid, D. Begue, P. Iratcabal, N. Redon, J. Desbrieres, S. Reynaud, Conducting polyaniline composite: from syntheses in waterborne systems to chemical sensor devices, *Polymer* 51 (2010) 1716–1722.
- [13] H. Okamoto, T. Kotaka, Structure and properties of polyaniline films prepared via electrochemical polymerization. I: Effect of pH in electrochemical Polymerization media on the primary structure and acid dissociation constant of product polyaniline films, *Polymer* 39 (1998) 4349–4358.
- [14] Y. Guo, Y. Zhou, Polyaniline nanofibers fabricated by electrochemical polymerization: a mechanistic study, *Eur. Polym. J.* 43 (2007) 2292–2297.
- [15] S. Mu, J. Kan, J. Lu, L. Zhuang, Interconversion of polarons and bipolarons of polyaniline during the electrochemical polymerization of aniline, *J. Electroanal. Chem.* 446 (1998) 107–112.
- [16] J. Zhang, L. Kong, B. Wang, Y. Luo, L. Kang, In-situ electrochemical polymerization of multi-walled carbon nanotube/polyaniline composite films for electrochemical supercapacitors, *Synth. Met.* 159 (2009) 260–266.
- [17] S.G. Pawar, S.L. Patil, M.A. Chougule, B.T. Raut, S.A. Pawar, R.N. Mulik, V.B. Patil, Nanocrystalline TiO₂ thin films for NH₃ monitoring: microstructural and physical characterization, *J. Mater. Sci.: Mater. Electron.* 23 (2012) 273–279.
- [18] S.H. Weng, J.Z. Zhou, Z.H. Lin, Preparation of one-dimensional (1D) polyaniline-polypyrrole coaxial nanofibers and their application in gas sensor, *Synth. Met.* 160 (2010) 1136–1142.
- [19] D.R. Miller, S.A. Akbar, P.A. Morris, Nanoscale metal oxide-based heterojunctions for gas sensing: a review, *Sens. Actuators B: Chem.* 204 (2014) 250–272.
- [20] M. Hubner, D. Koziej, M. Bauer, N. Barsan, K. Kvashnina, M.D. Rossell, U. Weimar, J.D. Grunwaldt, The structure and behavior of platinum in SnO₂-Based sensors under working conditions, *Angew. Chem. Int. Ed.* 50 (2011) 2841–2844.
- [21] Y.H. Li, J.A. Gong, G.H. He, Y.L. Deng, Synthesis of polyaniline nanotubes using Mn₂O₃ nanofibers as oxidant and their ammonia sensing properties, *Synth. Met.* 161 (2011) 56–61.
- [22] M.A. Chougule, S.G. Pawar, S.L. Patil, B.T. Raut, P.R. Godse, S. Sen, V.B. Patil, Polypyrrole thin film: room temperature ammonia gas sensor, *IEEE Sens. J.* 11 (2011) 2137–2141.
- [23] M.K. Ram, O. Yavuz, V. Lahsangah, M. Aldissi, CO gas sensing from ultrathin nano-composite conducting polymer film, *Sens. Actuators B: Chem.* 106 (2005) 750–757.
- [24] L.L. Wang, H. Huang, S.H. Xiao, D.P. Cai, Y. Liu, B. Liu, D.D. Wang, C.X. Wang, H. Li, Y.R. Wang, Q.H. Li, T.H. Wang, Enhanced sensitivity and stability of room-Temperature NH₃ sensors using core-Shell CeO₂ nanoparticles@Cross-linked PANI with p-n heterojunctions, *ACS Appl. Mater. Interfaces* 6 (2014) 14131–14140.
- [25] A.Z. Sadek, W. Włodarski, K. Shin, R. Bkaner, K. Kalantar-zadeh, Alayered surface acoustic wave gas sensor based on a polyaniline/In₂O₃ nanofibre composite, *Nanotechnology* 17 (2006) 4488–4492.
- [26] S. Nasirian, H.M. Moghaddam, Hydrogen gas sensing based on polyaniline/anatase titania nanocomposite, *Int. J. Hydrogen Energy* 39 (2014) 630–640.
- [27] P. Camagni, G. Faglia, P. Galinetto, C. Perego, G. Samoggia, G. Sberveglieri, Photosensitivity activation of SnO₂ thin film gas sensors at room temperature, *Sens. Actuators B: Chem.* 31 (1996) 99–103.
- [28] C. Cao, C. Hu, X. Wang, et al., UV sensor based on TiO₂ nanorod arrays on FTO thin film, *Sens. Actuators B: Chem.* 159 (2011) 114–119.
- [29] Q. Geng, Z.J. He, X. Chen, W.X. Dai, X.X. Wang, Gas sensing property of ZnO under visible light irradiation at room temperature, *Sens. Actuators B: Chem.* 118 (2013) 293–297.
- [30] Y.M. Lin, D.Z. Li, J.J. Hu, G.C. Xiao, J.X. Wang, W.J. Li, X.Z. Fu, Highly efficient photocatalytic degradation of organic pollutants by PANI-Modified TiO₂ composite, *J. Phys. Chem. C* 116 (2012) 5764–5772.
- [31] M. Radoičić, Ž. Šaponjić, I.A. Janković, G. Čirić-Marjanović, S.P. Ahrenkiel, M.I. Čomor, Improvements to the photocatalytic efficiency of polyaniline modified TiO₂ nanoparticles, *Appl. Catal. B* 136–137 (2013) 133–139.
- [32] X.Y. Peng, Z.J. He, K. Yang, X. Chen, X.X. Wang, W.X. Dai, X.Z. Fu, Correlation between donating or accepting electron behavior of the adsorbed CO or H₂ and its oxidation over TiO₂ under ultraviolet light irradiation, *Appl. Surf. Sci.* 360 (2016) 698–706.
- [33] K. Yang, K. Huang, Z.J. He, X. Chen, X.Z. Fu, W.X. Dai, Promoted effect of PANI as electron transfer promoter on CO oxidation over Au/TiO₂, *Appl. Catal. B: Environ.* 158–159 (2014) 250–257.
- [34] Q. Geng, X.H. Lin, R.R. Si, X. Chen, W.X. Dai, X.Z. Fu, X.X. Wang, The correlation between the ethylene response and its oxidation over TiO₂ under UV irradiation, *Sens. Actuators B: Chem.* 174 (2012) 449–457.
- [35] K. Yang, Y.X. Li, K. Huang, X. Chen, X.Z. Fu, W.X. Dai, Promoted effect of PANI on the preferential oxidation of CO in the presence of H₂ over Au/TiO₂ under visible light irradiation, *Int. J. Hydrogen Energy* 39 (2014) 18312–18325.
- [36] F. Deng, L.J. Min, X.B. Luo, S.L. Wu, S.L. Luo, Visible-light photocatalytic degradation performances and thermal stability due to the synergistic effect of TiO₂ with conductive copolymers of polyaniline and polypyrrole, *Nanoscale* 3 (2013) 8703–8710.
- [37] Y.S. Zhang, W.H. Xu, W.T. Yao, S.H. Yu, Oxidation-reduction reaction driven approach for hydrothermal synthesis of polyaniline hollow spheres with controllable size and shell thickness, *J. Phys. Chem. C* 113 (2009) 8588–8594.
- [38] G. Louarn, M. Lapkowski, S. Quillard, A. Pron, J.P. Buisson, S. Lefrant, Vibrational properties of polyaniline-isotope effects, *J. Phys. Chem.* 100 (1996) 6998–7006.
- [39] N. Serpone, D. Lawless, R. Khairutdinov, Size effect on the photophysical properties of colloidal anatase TiO₂ particles: size quantization or direct transitions in this indirect semiconductor, *J. Phys. Chem.* 99 (1995) 16646–16654.
- [40] S. Deivanayaki, V. Ponnuswamy, S. Ashokan, P. Jayamurugan, R. Mariappan, Synthesis and characterization of TiO₂-doped polyaniline nanocomposites by chemical oxidation method, *Mater. Sci. Semicond. Process.* 16 (2013) 554–559.
- [41] H.M. Moghaddama, S. Nasiriana, Hydrogen gas sensing feature of polyaniline/titania (rutile)nanocomposite at environmental conditions, *Appl. Surf. Sci.* 317 (2014) 117–124.
- [42] Y. Cao, P. Smith, A.J. Heeger, Spectroscopic studies of polyaniline in solution and in spin-cast films, *Synth. Met.* 32 (1989) 263–281.
- [43] X.W. Li, G.C. Wang, X.X. Li, D.M. Lu, Surface properties of polyaniline/nano-TiO₂ composites, *Appl. Surf. Sci.* 229 (2004) 395–401.
- [44] A. Olad, S. Behboudi, A.A. Entezami, Preparation, characterization and photocatalytic activity of TiO₂/polyaniline core-shell nanocomposite, *Bull. Mater. Sci.* 35 (2012) 801–809.
- [45] Y. Guo, D. He, S. Xia, X. Xie, X. Gao, Q. Zhang, Preparation of a novel nanocomposite of polyaniline core decorated with anatase-TiO₂ nanoparticles in ionic liquid/water microemulsion, *J. Nanomater.* 2012 (2012) 1–7.
- [46] T. Ohsaka, F. Izumi, Y. Fujiki, Raman spectrum of anatase, TiO₂, *J. Raman Spectroscopy* 7 (1978) 321–324.
- [47] S.I. Seok, J.H. Kim, TiO₂ nanoparticles formed in silica sol-gel matrix, *Mater. Chem. Phys.* 86 (2004) 176–179.
- [48] X.Y. Li, D.S. Wang, G.X. Cheng, Q.Z. Luo, J. An, Y.H. Wang, Preparation of polyaniline-modified TiO₂ nanoparticles and their photocatalytic activity under visible light illumination, *Appl. Catal. B: Environ.* 81 (2008) 267–273.
- [49] W.C. Chen, T.C. Wen, A. Gopalan, The inductive behavior derived from hydrolysis of polyaniline, *Electrochim. Acta* 47 (2002) 4195–4206.
- [50] Y.Z. Li, Y. Yu, L.Z. Wu, J.F. Zhi, Processable polyaniline/titania nanocomposites with good photocatalytic and conductivity properties prepared via peroxo-titanium complex catalyzed emulsion polymerization approach, *Appl. Surf. Sci.* 273 (2013) 135–143.
- [51] B.T. Su, X.H. Liu, X.X. Peng, T. Xiao, Z.X. Su, Preparation and characterization of the TiO₂/polymer complex nanomaterial, *Mater. Sci. Eng.: A* 49 (2003) 59–62.
- [52] M.A. Centeno, M. Paulis, M. Montes, J.A. Odriozola, Catalytic combustion of volatile organic compounds on gold/titanium oxynitride catalysts, *Appl. Catal. B: Environ.* 61 (2005) 177–183.
- [53] E.T. Kang, K.G. Neoh, Y.K. Ong, K.L. Tan, B.T.G. Tan, X-ray photoelectron spectroscopic studies of polypyrrole synthesized with oxidative iron (III) salts, *Macromolecules* 24 (1991) 2822–2828.
- [54] T.H. Lee, J.W. Rabalais, X-ray photoelectron-spectra and electronic-structure of some diamine compounds, *J. Electron Spectrosc. Relat. Phenom.* 11 (1977) 123–127.
- [55] S.N. Kumar, F. Gaillard, G. Bouyssoux, A. Sartre, High-resolution XPS studies of electrochemically synthesized conducting polyaniline films, *Synth. Met.* 36 (1990) 111–127.
- [56] G. Sebastian, K. Anna, F. Mats, L. Krzysztof, J.L. Jerzy, *Solid. State. Ionics* 179 (2008) 2234–2239.

- [57] A.Z. Sadek, C.O. Baker, D.A. Powell, Polyaniline nanofiber based surface caustic wave gas sensors—effect of nanofiber diameter on H₂ response, *IEEE Sens. J.* 7 (2007) 213–218.
- [58] T.E. Olinga, J. Fraysse, J. Travers, A. Dufresne, A. Pron, Highly conducting and solution-processable polyaniline obtained via protonation with a new sulfonic acid containing plasticizing functional groups, *Macromolecules* 33 (2000) 2107–2113.
- [59] W.X. Dai, X. Chen, X.P. Zheng, Z.X. Ding, X.X. Wang, P. Liu, X.Z. Fu, Photocatalytic oxidation of CO on TiO₂: chemisorption of O₂, CO, and H₂, *ChemPhysChem* 10 (2009) 411–419.